Computers and Structures 222 (2019) 118–132

Contents lists available at ScienceDirect

Computers and Structures

journal homepage: www.elsevier.com/locate/compstruc

Nonlinear sectional analysis of reinforced concrete beams and shells subjected to pure torsion

Allan Kuan [a,*], Edvard P.G. Bruun [a,b], Evan C. Bentz [a], Michael P. Collins [a]

[a] Department of Civil and Mineral Engineering, Faculty of Applied Science and Engineering, University of Toronto, 35 St. George Street, M5S 1A4 Toronto, Ontario, Canada
[b] Department of Civil and Environmental Engineering, Princeton University, 59 Olden St., Princeton, NJ 08540, USA

ARTICLE INFO

Article history:
Received 1 November 2018
Accepted 1 July 2019

Keywords:
Reinforced concrete
Torsion
Beams
Shells
Sectional analysis
Nonlinear analysis

ABSTRACT

This paper presents a sectional analysis tool which can compute the complete torque-twist behaviour of reinforced concrete beams and shells. The cross section is modelled as a 2-D grid of triaxial elements representing the concrete and uniaxial elements representing the longitudinal reinforcement. Fixed strain patterns based on kinematic assumptions are used instead of using the finite element method to calculate strain distributions corresponding to sectional strains. Constitutive models for the concrete are based on the Modified Compression-Field Theory, though tension stiffening is neglected in the proposed model's current implementation. A key assumption used in this model is that the shear strain distribution caused by twists obtained from a linear elastic analysis can be used to describe the nonlinear behaviour of a member following cracking. The validity of this assumption when applied to rectangular sections is confirmed based on a study of 115 tests from the literature. Excellent agreement of peak strength and overall torque-twist behaviour are observed when comparing the model predictions and experimental data from these tests. Areas of future work are to improve the capabilities of the model are identified.

1. Torsion in reinforced concrete structures

In the design or analysis of a reinforced concrete structure, the ability of its members to carry torsion and resist twisting displacements needs to be considered. Common instances in which torsion is particularly important include bridges curved in space or spandrel beams in buildings – for members such as these, the torsion is predominantly carried by shear stresses which circulate around the member's cross section. As the tensile strength of concrete is low, even small torsions can cause the formation of diagonal cracks which then spiral around the member. These cracks lead to a dramatic reduction in the torsional stiffness of the member, which may lead to a redistribution of how the loads are carried by the overall structure. The cracking also alters how the torsion is resisted by the member, with the circulating shear stresses now being carried by fields of diagonal compression in the cracked concrete which are equilibrated by tensile forces carried by transverse and longitudinal reinforcement.

The post-cracking response of reinforced concrete members has important implications for both the global behaviour of the overall structure and the local behaviour of the member carrying the torsion. In statically indeterminate structures, the reduction in torsional stiffness following cracking leads to redistribution in the loads throughout the structure as the cracked member continues twisting in order to maintain compatibility. In statically determinate structures where the load path does not change following cracking, the torsional strength of the cracked member is required to be large enough so that equilibrium is maintained in the structure to avoid collapse. These two phenomena were identified by Collins and Lampert in 1973 as Compatibility Torsion and Equilibrium Torsion respectively [1]. To account for these two types of torsion, an engineer would benefit from knowing how the stiffness of the member changes following cracking, whether or not the member is able to achieve large twists without failing, and what the member's strength is when resisting torsion in combination with axial loads, shears and moments. These requirements naturally call for practical nonlinear analysis tools which can reliably predict the full torque-twist behaviour of reinforced and prestressed concrete members.

1.1. Challenges with numerical modelling of reinforced concrete members subjected to torsion

Modelling the behaviour of reinforced concrete members subjected to torsion is inherently a 3-D problem, as torsion is not present when conducting a 2-D analysis of a structure or member. The

* Corresponding author.
E-mail address: allan.kuan@mail.utoronto.ca (A. Kuan).

https://doi.org/10.1016/j.compstruc.2019.07.001
0045-7949/

current state-of-the-art for dealing with torsion in reinforced concrete members makes use of finite element methods in tandem with nonlinear constitutive models. These approaches can be largely grouped into using solid elements to model portions of structures, an example being VecTor3 developed at the University of Toronto by Vecchio and Selby [2] (shown in Fig. 1), or using frame elements whose stiffnesses are derived from a finite element analysis of the kinematic behaviour of member's cross section (such as methods developed by Bairan and Mari [3], Capdevielle et al. [4] and Gregori et al. [5]).

The strength of these approaches is that the response of arbitrarily shaped members can be modelled in great detail, with previous validation studies demonstrating their ability to accurately predict the torque-twist response of experiments found in the literature. However, their feasibility for practical application is limited by the large computational resources required to conduct an analysis. The costs of constructing and inverting a large global stiffness matrix can be very high, particularly when working the large meshes associated with using solid elements. The process is made even more challenging when modelling nonlinear behaviour, as many of the sophisticated constitutive models for the cracked concrete require iteration to converge on material stiffnesses at each load step. To avoid prohibitively long runtimes, a coarse mesh in the numerical model may be needed when using these methods, which detracts from the intended benefits offered by these models.

1.2. Sectional analysis of reinforced concrete members

Sectional analysis methods characterize the behaviour of a member by analyzing the behaviour of the cross section when subjected to stress resultants such as axial load, shear, moment and torsion. These methods, similar in approach to the layered analysis in fiber models, can quickly perform detailed calculations across a cross section because a global stiffness matrix does not need to be assembled and inverted. Response-2000 by Bentz, shown schematically in Fig. 2, is a widely used example of a sectional analysis program for reinforced concrete members [6]. Plane sections are assumed to remain plane after deformation, the shear strain distribution is calculated by considering equilibrium between the fibers and the Modified Compression-Field Theory (MCFT) is used as a constitutive model for the concrete stress-strain behaviour [7]. Unfortunately, Response-2000 cannot account for torsion as it is only formulated to obtain the response caused by combinations of axial load, moment and shear.

Sectional analysis programs which can account for torsion in combination with axial load, bending and shear typically make use of a space truss model, which represents the cross section as a space truss with four chords and four webs arranged in a rectangular shape. Bredt's simple equation for thin-walled tubes is typically used to estimate the shear flows caused by torsion, instead of a more detailed approach. An example of a space truss model which uses the MCFT is COMBINED, developed by Rahal and Collins [8] and shown in Fig. 2. Other models in the literature such as the Softened Membrane Model for Torsion (SMMT) by Jeng and Hsu [9], the Combined-Action Softened Truss Model (CA-STM) by Green and Belarbi [10] and the Modified Variable Angle Truss-Model (MVATM) by Bernardo et al. [11] similarly use a space truss approach, albeit using different constitutive relationships for concrete and steel. Although these space truss models are computationally efficient, their simplifications (such as using Bredt's equation and representing of the actual section as a rectangular truss) mean that rigorously modelling arbitrarily shaped members is more difficult compared using to the finite element approaches mentioned in Section 1.1, and less information can be ascertained about how the member is carrying the torsion.

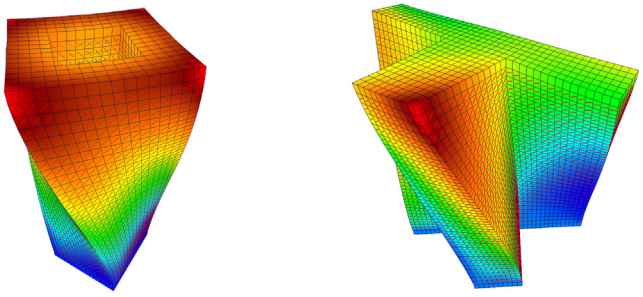

Fig. 1. Sample output from a VecTor3 analysis for a hollow box (left) and T-section (right) subjected to pure torsion.

2. Proposed analysis model

The proposed analysis model described in this paper is a sectional analysis tool for obtaining the response of reinforced and prestressed concrete members in pure torsion. The model combines the strengths of the finite element methods discussed in Section 1.1 with the lower computational requirements of the sectional analysis methods discussed in Section 1.2. While currently implemented to only calculate the behaviour of rectangular sections in pure torsion, the methodology can be extended to account for the response of a general cross section shape subject to the six sectional stress resultants (axial load N_z, vertical shear V_y, lateral shear V_x, vertical moment M_x, lateral moment M_y and torque T_z, defined using the notation shown on the space truss model in Fig. 2).

2.1. General framework and methodology

To perform the analysis, the following steps are taken. These steps are presented at a high level and are described in further detail in Sections 2.1–2.4 and summarized in Section 2.5 which

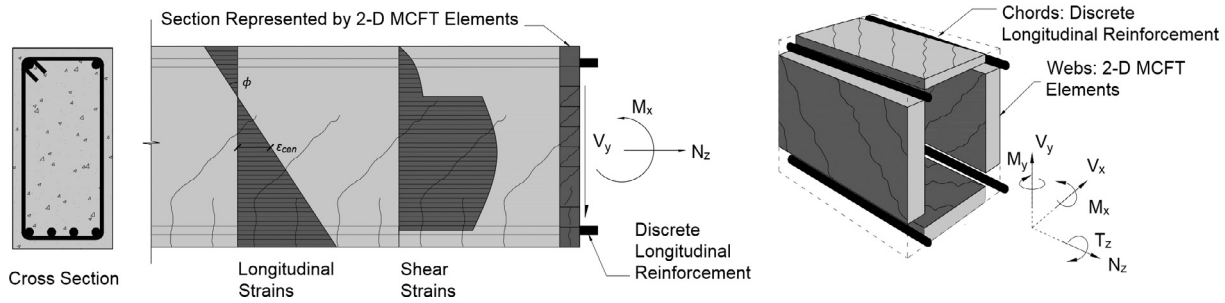

Fig. 2. Representations of the cross section of a reinforced concrete member in Response-2000 (left) and using a space-truss model such as COMBINED (right).

illustrates the special case of applying the general procedure for obtaining the torque-twist response of a member in pure torsion.

(1) Create a representation of the cross section in the *x*-*y* plane using a 2-D grid of elements which represents the reinforced concrete and steel reinforcement materials.
(2) Calculate strain distributions which correspond to the six possible sectional strains.
(3) Specify a desired ratio of (N_z, V_y, V_x, M_x, M_y, T_z) that the section will carry.
(4) Specify a sectional strain value which will guide the analysis. For pure torsion, this is the twist, ψ_z.
(5) Apply a set of sectional strains. Using the strain distributions calculated in step 2, calculate the longitudinal strain ε_z and shear strains γ_{zy} and γ_{zx} in each element in the cross section.
(6) Calculate the distribution of axial and shear stresses in the cross section using the material constitutive relationships.
(7) Integrate the stresses across the cross section to calculate the global section stress resultants. If the ratio of stress resultants does not match what was specified in step 3, modify the proportion of sectional strains in an iterative manner until convergence is achieved.
(8) Increment the guiding sectional strain in step 4 and repeat steps 5–7 until the analysis is completed.

Representing the cross section in the model is done by discretizing the cross section into uniaxial elements, which represent the longitudinal reinforcement, and triaxial elements, which represent the reinforced concrete with embedded transverse reinforcement. Sample discretization for a hollow beam and a slab strip or shell element are shown in Fig. 3. Although these components are described as elements, the model does not use the finite element method as no global stiffness matrix is assembled and shape functions are not used to describe how degrees of freedom in each element interact with one another. Instead, each element is simply a calculation point where the element stresses are calculated given the strains at that point. Stress resultants are calculated by integrating the element stresses over its area, $A_{element}$.

The distribution of longitudinal axial strains and shear strains throughout the cross section are obtained by using fixed strain distributions which correspond to each of the six sectional strains and are explained in further detail in Section 2.2. These sectional strains are the centroidal axial strain, ε_{z0}, the centroidal vertical shear strain, γ_{zy0}, the centroidal lateral shear strain, γ_{zx0}, the vertical curvature, ϕ_x, the lateral curvature, ϕ_y and the twist, ψ_z. The benefits of using fixed strain patterns is that element strains can be directly computed given the sectional strains instead of being derived from a finite element analysis, which allows the section to be finely discretized while maintaining a reasonable analysis runtime.

Constitutive relationships used for modelling the triaxial stress-strain behaviour for reinforced concrete and the uniaxial stress-strain behaviour for conventional and prestressed reinforcement are presented in Section 2.3. Although these models are used in the current implementation, the framework is flexible enough to accommodate any constitutive models for the reinforced concrete and steel materials.

It should be noted that the model is currently implemented to only handle pure torsion and hence the associated strain distributions for γ_{zy0} and γ_{zx0}, which are associated with V_y and V_x, are not used. Their derivation remains an area of future work as the framework is developed further. However, the steps described in the above procedure are general enough to completely describe how to perform an analysis involving all six stress resultants if these distributions are known.

2.2. Assumed strain distributions

To perform the analysis, the proposed model uses fixed strain patterns corresponding to each sectional strain to evaluate the axial and shear strains over the entire cross section. This means that given a set of sectional strains (ε_{z0}, γ_{zy0}, γ_{zx0}, ϕ_x, ϕ_y, ψ_z), the element strains (ε_z, γ_{zy},γ_{zx}) can be calculated at each point in the cross section. These strains are then used to evaluate the axial stresses f_z and shear stresses v_{zy} and v_{zx} in each element which produce the six sectional stress resultants when integrated over the cross section. Although these three element strains are sufficient for sectional analysis with linear elastic materials, for orthotropic materials such as cracked reinforced concrete, six strains are required to obtain a complete strain state and maintain equilibrium in each element in the section. These additional strains which describe how the cross section distorts, (ε_x, ε_y, γ_{xy}), are calculated once the concrete has begun to crack and nonlinear behaviour begins.

2.2.1. Longitudinal strains

Longitudinal axial strains are calculated using a linear strain profile per the Euler-Bernoulli plane sections hypothesis first described by Hooke in 1678 [12]. The strains are calculated as:

$$\varepsilon_z(x,y) = \varepsilon_{z0} - y\phi_x + x\phi_y \tag{1}$$

where ε_{z0} is the axial strain at the centroid of the cross section, ϕ_x is the vertical curvature causing flexural compression on the top of the beam and ϕ_y is the lateral curvature causing flexural compression on the left side of the beam.

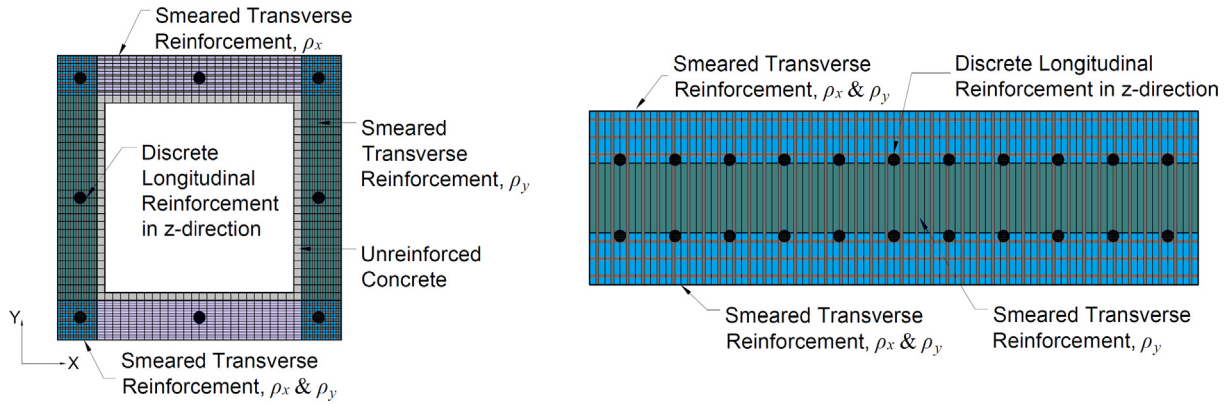

Fig. 3. Cross section discretization of a hollow beam (left) and slab strip or shell (right). Coloured rectangular elements are triaxial reinforced concrete elements and black circles are uniaxial reinforcement elements. The section is defined in the X-Y plane, with the z-direction being the longitudinal direction.

2.2.2. Shear strains caused by twist

Shear strains caused by twist are calculated using St. Venant's assumption that when twisted, a member warps in the longitudinal direction and the projection of the cross section onto a surface perpendicular to its axis rotates as a rigid body. If this warping is not restrained, the resulting torsion is resisted by circulatory shear stresses (which contrasts with torsion carried by axial stresses caused by restrained warping, referred to as warping torsion). By assuming that the warping is constant along the length of the member, the resulting shear strain distribution in the cross section is described by the following equations:

$$\gamma_{zy}(x,y) = \psi_z\left((x - x_o) + \frac{\partial \varphi_w(x,y)}{\partial y}\right) \tag{2}$$

$$\gamma_{zx}(x,y) = \psi_z\left(-(y - y_o) + \frac{\partial \varphi_w(x,y)}{\partial x}\right) \tag{3}$$

where γ_{zy} and γ_{zx} are the vertical and lateral engineering shear strains respectively, ψ_z is the twist, (x_o, y_o) are the coordinates of the shear centre and φ_w is a function describing the warping of the cross section.

Calculating the shear strain distribution of the cross section assuming linear elastic behaviour can be done using Prandtl's stress function approach and using an assumed material shear modulus G of unity:

$$\frac{\partial^2 \phi^*(x,y)}{\partial x^2} + \frac{\partial^2 \phi^*(x,y)}{\partial y^2} = -2\psi_z \tag{4}$$

where ϕ^* is the stress function related to the shear strains as shown below:

$$\gamma_{zx}(x,y) = \frac{\partial \phi^*(x,y)}{\partial y} \tag{5}$$

$$\gamma_{zy}(x,y) = -\frac{\partial \phi^*(x,y)}{\partial x} \tag{6}$$

Eq. (4) can be easily solved using a finite difference or finite element solution scheme given the boundary condition that ϕ^* is a constant along the boundary. As the method makes no assumption of the geometry of the member, the resulting distribution of strains can be determined for an arbitrarily shaped solid or hollow cross section. Plots of the stress function solution ϕ^* and resulting shear strain distributions for a solid square cross section, a hollow square cross section and a T-section are shown in the first two columns of Fig. 4.

A key assumption in the method proposed in this paper is that the member warps in the same manner both before and after cracking, resulting in the same pattern of shear strains caused by twisting. In reality, warping of a cracked reinforced concrete section is a complex phenomenon affected by the geometry of the member, the layout of reinforcement, the anisotropy of the concrete, the distribution of stiffness and the presence of accompanying stress resultants such as axial load, moment, shear and torsion. However, it has been found that for symmetrically reinforced members loaded in pure torsion, using this simplifying assumption allows reasonable prediction of the complete nonlinear response be obtained in a computationally efficient manner.

To validate this approach, a series of analyses were performed using VecTor3, a nonlinear finite element analysis software which uses 3-D solid elements and has previously been shown to give good results when modelling members carrying torsion [2]. The resulting shear strain distributions for cracked symmetrically reinforced members with solid square, hollow square and T-shaped cross sections are shown in the third column of Fig. 4. Comparing the elastic strain distributions with the inelastic strain distributions obtained using VecTor3, there is good agreement in the overall trends present. For the square sections, the regions of high shear strains are the same, and both models agree that the outside corners are areas of low shear strain. For the T-shape, the strain concentration around the re-entrant corners are present in both models, and again there is good agreement between the two regarding the regions of high and low shear strain.

The proposed methodology works best for members which are symmetrically reinforced and loaded in pure torsion. This is because the post-cracking distribution of stiffness is similar to that of the uncracked section, resulting in a similar pattern of warping being present. It becomes less appropriate for members whose warping changes substantially following cracking. Examples of when this occurs include when the member is non-symmetrically reinforced, which results in the member curving after cracking, or when the section is not uniformly cracked while being twisted (which occurs when torsion is present in combination with bending and/or shear) – the resultant non-uniform distribution of stiffness results in changes to the pattern of warping. However, validation of the model under combined torsion and bending in Section 4 demonstrates that reasonable results are still attainable even when these idealized conditions are not present.

2.2.3. Section distortion strains

A common assumption in beam theories for linear elastic materials, such as the bending of bars illustrated by Timoshenko, is that the cross section is rigid and neither expands, described by transverse axial strains ε_x and ε_y, nor distorts, described by in-plane shear strains γ_{xy} [13]. In elasticity, these geometric assumptions result in the assumption that the transverse clamping stresses f_x and f_y and the in-plane shear stress v_{xy} are equal to zero. However, reinforced concrete members need to expand following cracking in order to engage the transverse reinforcement and hence satisfy equilibrium when carrying shear stresses.

In the current implementation, distortion strains are obtained by assuming that $f_x = f_y = v_{xy} = 0$ at all points in the cross section and calculating $(\varepsilon_x, \varepsilon_y, \gamma_{xy})$ in order to satisfy this condition. For a 3-D constitutive model, this results in reducing the material constitutive matrix $[D]$ from a 6×6 matrix, notated as follows:

$$\begin{bmatrix} f_x \\ f_y \\ f_z \\ v_{xy} \\ v_{zy} \\ v_{zx} \end{bmatrix} = [D]_{6\times6} \begin{bmatrix} \varepsilon_x \\ \varepsilon_y \\ \varepsilon_z \\ \gamma_{xy} \\ \gamma_{zy} \\ \gamma_{zx} \end{bmatrix} \tag{7}$$

To a reduced 3×3 formulation:

$$\begin{bmatrix} f_z \\ v_{zy} \\ v_{zx} \end{bmatrix} = [D^*]_{3\times3} \begin{bmatrix} \varepsilon_z \\ \gamma_{zy} \\ \gamma_{zx} \end{bmatrix} \tag{8}$$

Here, $[D^*]$ is the reduced constitutive matrix which is derived by condensing the original constitutive matrix $[D]$ using the aforementioned assumptions on f_x, f_y and v_{xy}. The distortion strains can be then expressed as a linear combination of the section axial and shear strains using the following relationship:

$$\begin{bmatrix} \varepsilon_x \\ \varepsilon_y \\ \gamma_{xy} \end{bmatrix} = -[r]_{3\times3} \begin{bmatrix} \varepsilon_z \\ \gamma_{zy} \\ \gamma_{zx} \end{bmatrix} \tag{9}$$

where $[r]$ is a reduction matrix obtained when the converting the original 6×6 constitutive matrix $[D]$ to the 3×3 $[D^*]$. Sample expansion and distortion strains calculated when analyzing a

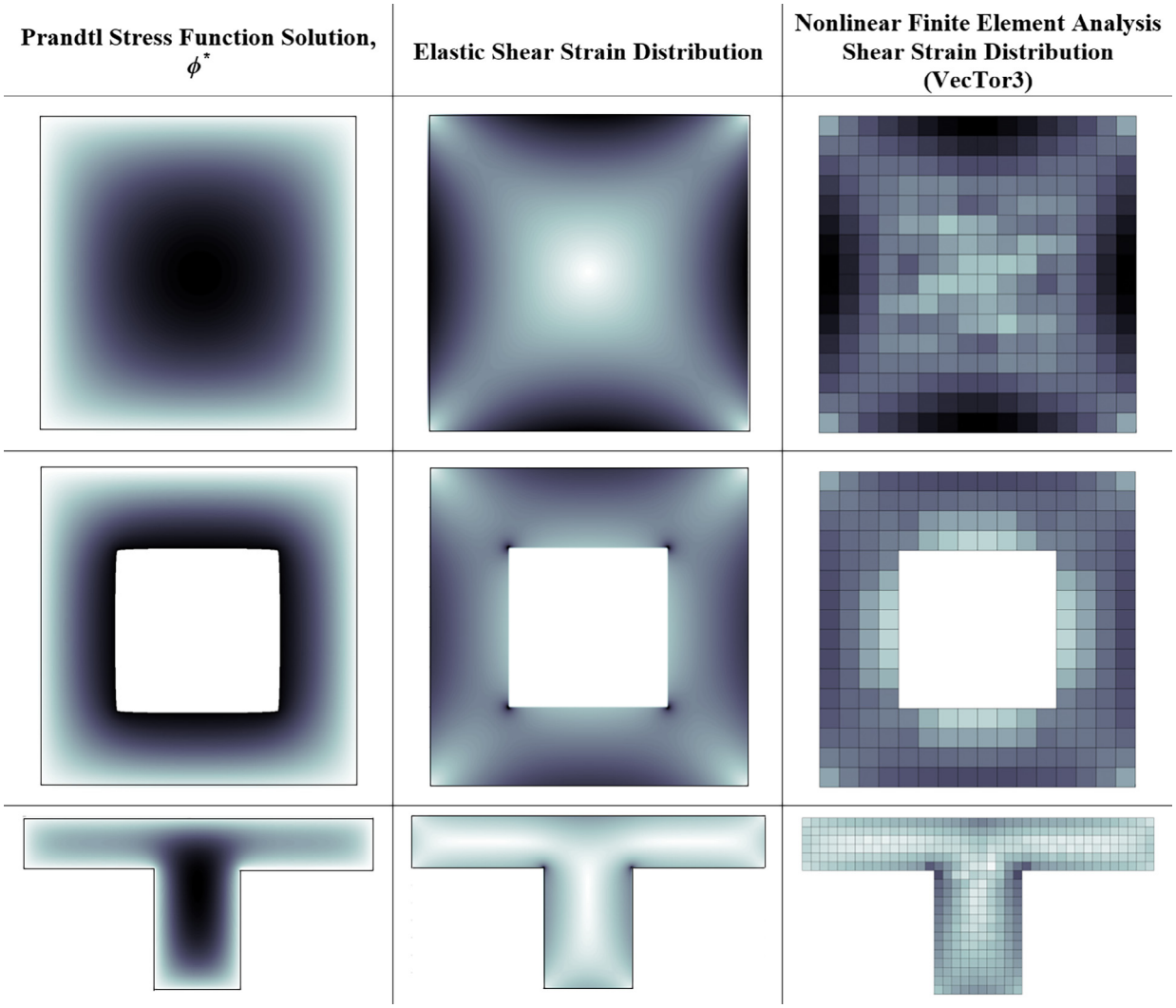

Fig. 4. Comparison of shear strain distributions caused by twist for solid square, hollow square and T-shaped cross sections. Darker colours indicate a larger magnitude of ϕ^* or γ.

symmetrically reinforced rectangular cross section in pure torsion which is fully cracked are shown in Fig. 5.

2.3. Constitutive modelling

The proposed analysis methodology requires constitutive models describing the triaxial behaviour of reinforced concrete and uniaxial behaviour of reinforcing and prestressing steel. Fig. 6 summarizes the constitutive models for concrete and steel which were used for the current implementation of the model. It should be noted that although the following subsections describe these models in greater detail, any constitutive models which meet these requirements may be used within the overall analysis framework.

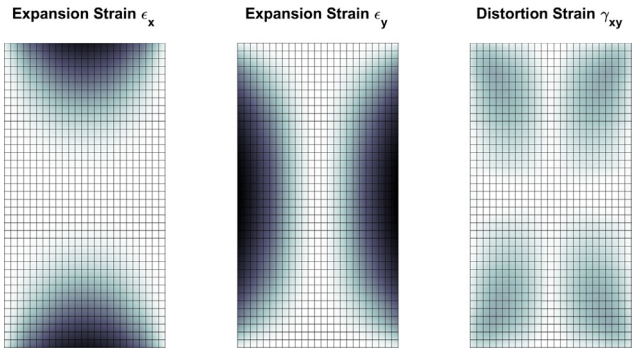

Fig. 5. Example expansion strains (horizontal, ε_x and vertical, ε_y) and distortion strains for a cracked section subjected to pure torsion. Darker colours indicate a higher magnitude of strain.

2.3.1. Reinforced concrete

Reinforced concrete elements are used to model all parts of the cross section apart from the longitudinal steel. Fig. 7 shows a representation of a typical reinforced concrete element containing transverse reinforcement. This reinforcement is smeared into the concrete element, with the quantity of reinforcement in each element with dimensions len_x by len_y being:

$$\rho_x = \frac{A_{s,x}}{s_z len_y} \tag{10}$$

$$\rho_y = \frac{A_{s,y}}{s_z len_x} \tag{11}$$

where $A_{s,x}$ and $A_{s,y}$ are the area of transverse steel assigned to the element in the x- and y- directions respectively and s_z is the spacing of this transverse reinforcement in the longitudinal direction.

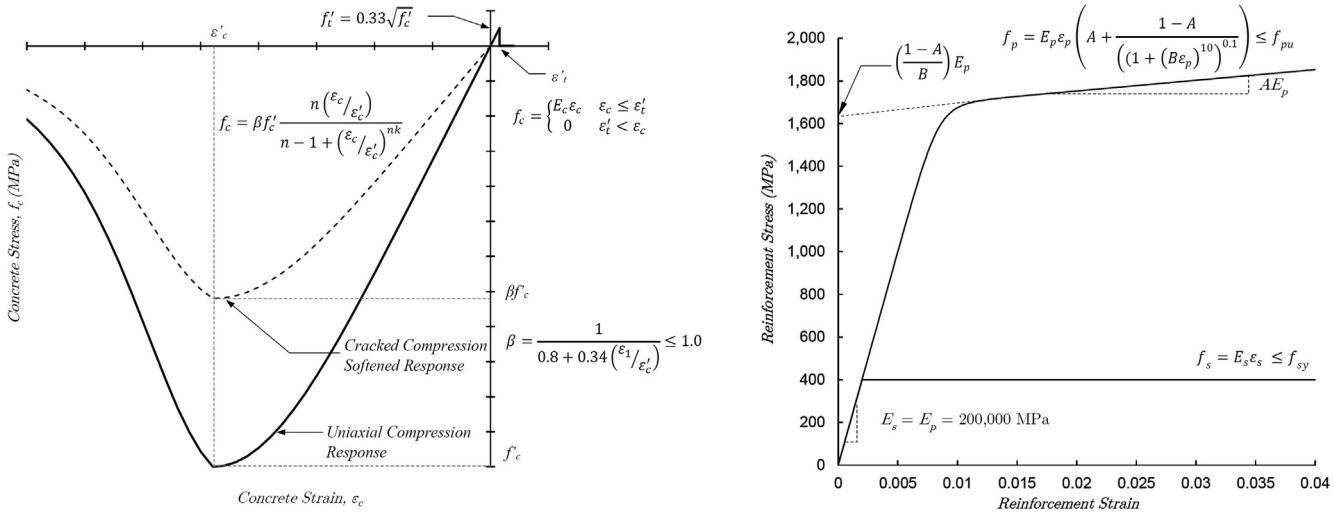

Fig. 6. Constitutive relationships for concrete (left) and steel reinforcement (right).

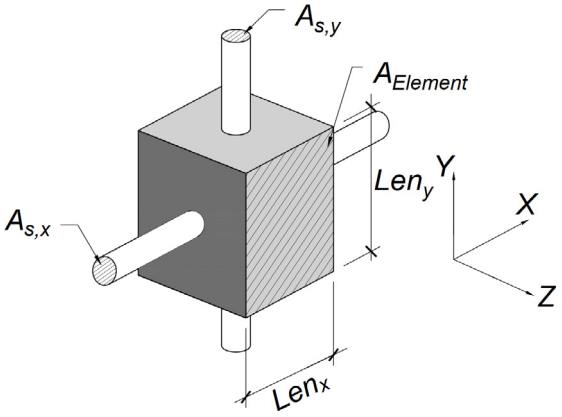

Fig. 7. Reinforced concrete element notation.

Although the method for smearing the reinforcement is smeared throughout the cross section is at the discretion of the user, smearing the steel mostly around the perimeter of the cross section – as shown in the hollow box in Fig. 3 – is the most realistic representation of the transverse reinforcement when performing a torsional analysis. More discussion on the smearing methodology when performing the analyses described in the paper is included in Section 3.

Prior to cracking, the concrete is treated as an isotropic linear elastic material and the smeared reinforcement has little effect on the overall behaviour. In the absence of provided test data, the Young's modulus of the concrete, E_c, the cracking stress f_t' and the cracking strain ε_t' can be calculated as [14]:

$$E_c = 3320\sqrt{f_c'} + 6900 \tag{12}$$

$$f_t' = 0.33\sqrt{f_c'} \tag{13}$$

$$\varepsilon_t' = \frac{f_t'}{E_c} \tag{14}$$

where E_c, f_t' and f_c', the cylinder compressive strength, are in MPa units.

Following cracking however, the cracked concrete is modelled as an orthotropic material with stiffnesses defined in its principal directions. A rotating crack model is used where the inclination of the principal stresses is assumed to coincide with the inclination of the principal strains in the same manner as the Modified Compression-Field Theory [7] and Poisson effects are neglected after cracking [2]. Thus, the principal stresses in the cracked concrete are evaluated using the principal strains in the element.

The constitutive matrix of the cracked reinforced concrete, $[D]$, is defined as:

$$[D] = [D_c] + [D_s] \tag{15}$$

where $[D_c]$ and $[D_s]$ are the constitutive matrices for the cracked concrete and steel respectively:

$$[D_c] = [T_c]^T \begin{bmatrix} \bar{E}_{c1} & 0 & 0 & 0 & 0 & 0 \\ 0 & \bar{E}_{c2} & 0 & 0 & 0 & 0 \\ 0 & 0 & \bar{E}_{c3} & 0 & 0 & 0 \\ 0 & 0 & 0 & \frac{\bar{E}_{c1}\bar{E}_{c2}}{\bar{E}_{c1}+\bar{E}_{c2}} & 0 & 0 \\ 0 & 0 & 0 & 0 & \frac{\bar{E}_{c2}\bar{E}_{c3}}{\bar{E}_{c2}+\bar{E}_{c3}} & 0 \\ 0 & 0 & 0 & 0 & 0 & \frac{\bar{E}_{c1}\bar{E}_{c3}}{\bar{E}_{c1}+\bar{E}_{c3}} \end{bmatrix} [T_c] \tag{16}$$

$$[D_s] = \begin{bmatrix} \rho_x\bar{E}_{sx} & 0 & 0 & 0 & 0 & 0 \\ 0 & \rho_y\bar{E}_{sy} & 0 & 0 & 0 & 0 \\ 0 & 0 & 0 & 0 & 0 & 0 \\ 0 & 0 & 0 & 0 & 0 & 0 \\ 0 & 0 & 0 & 0 & 0 & 0 \\ 0 & 0 & 0 & 0 & 0 & 0 \end{bmatrix} \tag{17}$$

where $[T_c]$ is the rotation matrix containing direction cosines (l_i, m_i, n_i) from x-y-z coordinates to the principal directions *1-2-3* [15] and $\bar{E}$ is the secant modulus of the concrete or steel, defined as the ratio of the material stress component f_i divided by its component of total strain ε_i:

$$[T_c] = \begin{bmatrix} l_1^2 & m_1^2 & n_1^2 & l_1m_1 & m_1n_1 & n_1l_1 \\ l_2^2 & m_2^2 & n_2^2 & l_2m_2 & m_2n_2 & n_2l_2 \\ l_3^2 & m_3^2 & n_3^2 & l_3m_3 & m_3n_3 & n_3l_3 \\ 2l_1l_2 & 2m_1m_2 & 2n_1n_2 & l_1m_2+l_2m_1 & m_1n_2+m_2n_1 & n_1l_2+n_2l_1 \\ 2l_2l_3 & 2m_2m_3 & 2n_2n_3 & l_2m_3+l_3m_2 & m_2n_3+m_3n_2 & n_2l_3+n_3l_2 \\ 2l_3l_1 & 2m_3m_1 & 2n_3n_1 & l_3m_1+l_1m_3 & m_3n_1+m_1n_3 & n_3l_1+n_1l_3 \end{bmatrix} \tag{18}$$

$$\bar{E}_i = \frac{f_i}{\varepsilon_i} \tag{19}$$

The stress-strain behaviour of the concrete in compression is modelled using Popovic's formulation [16], shown below:

$$f_c(\varepsilon_c) = \beta f_c' \frac{n(\varepsilon_c/\varepsilon_c')}{n - 1 + (\varepsilon_c/\varepsilon_c')^{nk}} \tag{20}$$

where f_c' is the cylinder crushing strength of the concrete, ε_c' is the strain corresponding to the peak compressive stress, n is a fitting parameter and k is a parameter which accounts for the loss of post-peak ductility in high strength concrete. Equations for n, k and ε_c' based on f_c' in MPa units are [16,17]:

$$n = 0.8 + \frac{f_c'}{17} \tag{21}$$

$$k = \begin{cases} 1.0 & \varepsilon_c/\varepsilon_c' < 1.0 \\ 0.67 + \frac{f_c'}{62} \geq 1.0 & 1.0 \leq \varepsilon_c/\varepsilon_c' \end{cases} \tag{22}$$

$$\varepsilon_c' = \frac{f_c'}{E_c}\frac{n}{n-1} \tag{23}$$

Due to the presence of tensile strains in the cracked concrete, the compression response is modified by a compression softening parameter β which accounts for the reduction in strength and stiffness of cracked concrete caused by the principal tensile strain ε_1. The formulation used for β is the expression used by Vecchio and Selby which is [2]:

$$\beta = \frac{1}{0.8 + 0.34(\varepsilon_1/\varepsilon_c')} \leq 1.0 \tag{24}$$

In tension, it is assumed that the concrete does not carry any tensile stress after cracking occurs (i.e. the tension stiffening effect is neglected). This can be represented as:

$$f_c = \begin{cases} E_c\varepsilon_c & 0 \leq \varepsilon_c \leq \varepsilon_t' \\ 0 & \varepsilon_t' \leq \varepsilon_c \end{cases} \tag{25}$$

This simplified constitutive model for concrete in tension was selected for two main reasons. The first reason is the lack of validated tension stiffening models which account for how the distribution of reinforcement affects the distribution of tensile stresses in the cracked concrete. Several approaches have been proposed in the past: Bentz modifies the basic tension stiffening expression in the MCFT by accounting for bond, though its application is limited to 2-D sectional analysis [18]. Proestos similarly introduces a modification factor for concrete elements to reduce the tension stiffening away from reinforcement [19]. In the VecTor suite of finite element programs developed at the University of Toronto, concrete located within a distance of 7.5 times the bar diameter around the reinforcement is assumed to use the Bentz tension stiffening model and tension softening equations are used beyond that [20]. Although these approaches have been shown to work well for their respective applications, a rigorous method for 3-D sectional analysis that has been validated against experimental data is not yet available for use.

The second reason for using a simplified approach is due to the difficulty of implementing a crack check to limit the tensile stresses in the concrete once the reinforcement begins to yield or when aggregate interlock breaks down. As explained by Vecchio and Collins [7] and later illustrated by Bentz [6], the average tensile stresses in the reinforced concrete must be limited by local behaviour at a crack. Neglecting this check can be dangerous as it leads to overestimating the strength of a members whose behaviour are controlled by yielding. Although Bentz describes a method for reducing the tensile stresses upon yield for a 2-D sectional analysis, an analogous procedure for limiting the tensile stresses in the concrete for 3-D sectional analysis remains an area of future work.

This simple assumption of neglecting post-cracking tensile stresses results in a model which tends to under-predict the torsional stiffness after cracking and conservatively estimate the strength of members whose torsional capacity is significantly influenced by tension in the concrete after cracking. This second case may occur in beams which contain large amounts of longitudinal steel and small amounts of transverse steel, as the tensile stresses in the concrete may account for a large proportion of the overall tensile stresses in the cracked member at failure. However, for beams which fail due to yielding of both directions of steel (a case where yielding of the steel at the crack controls the response at failure) or whose peak load are governed by crushing of the concrete, accurate results can still be obtained by using this simple constitutive relationship.

2.3.2. Reinforcing steel

Conventional reinforcement – either the transverse steel smeared into the reinforced concrete elements or the longitudinal reinforcement – is modelled as having an elastic-plastic stress-strain response, with strain hardening being neglected. The following equation is used for bars in tension and an analogous expression is used for bars in compression:

$$f_s = E_s\varepsilon_s \leq f_{sy} \tag{26}$$

where f_s is the is the reinforcement stress, E_s is the Young's modulus of the steel taken to be 200,000 MPa, ε_s is the steel strain and f_{sy} is the yield stress. Note that dowel action is neglected and perfect bond between the reinforcement and the surrounding concrete is assumed.

2.3.3. Prestressing steel

For prestressing steel, a modified Ramberg-Osgood formulation is used as recommended by Collins and Mitchell [14]. The stress-strain expression is as follows:

$$f_p = E_p\varepsilon_p\left(A + \frac{1-A}{\left(1 + (B\varepsilon_p)^{10}\right)^{0.1}}\right) \leq f_{pu} \tag{27}$$

where E_p is the initial Young's modulus of the steel, typically taken as 200,000 MPa and f_{pu} is the ultimate stress of the reinforcement. Definitions of A and B, fitting parameters which describe the post-yielding stiffness and yield stress respectively, are shown in Fig. 6. In lieu of experimentally obtained values, Collins and Mitchell suggest values of 0.025 and 118 for A and B respectively for low-relaxation strand [14].

To account for the prestress in the steel, a strain difference $\Delta\varepsilon_p$ is used to offset the strain in the prestressing steel from the strain in the surrounding concrete:

$$\varepsilon_p = \varepsilon_c + \Delta\varepsilon_p \tag{28}$$

where ε_c is the strain in the surrounding concrete.

2.4. Calculating stress resultants and obtaining torque-twist behaviour

Once the strains have been obtained over the cross section and the stresses at each element been calculated, the section stress resultants can be computed using the following formulas:

$$N_z = \int f_z dA_c + \int f_s dA_s + \int f_p dA_p \tag{29}$$

$$V_y = \int v_{zy} dA_c \tag{30}$$

$$V_x = \int v_{zx} dA_c \tag{31}$$

$$M_x = \int (y - y_{cen}) f_z dA_c + \int (y - y_{cen}) f_s dA_s + \int (y - y_{cen}) f_p dA_p \tag{32}$$

$$M_y = \int (x - x_{cen}) f_z dA_c + \int (x - x_{cen}) f_s dA_s + \int (x - x_{cen}) f_p dA_p \tag{33}$$

$$T_z = \int \left((x - x_o) v_{zy} - (y - y_o) v_{zx} \right) dA_c \tag{34}$$

where (x_{cen}, y_{cen}) are the coordinates of the section centroid, (x_o, y_o) are the coordinates of the shear centre, A_c is the area of reinforced concrete elements, A_s is the area of discrete longitudinal reinforcement and A_p is the area of discrete prestressed steel reinforcement.

2.5. Model implementation for pure torsion

The proposed model has been implemented in a MATLAB script, and is currently formulated to model the behaviour of solid and hollow reinforced and prestressed concrete members with a rectangular cross section. Fig. 8 shows the general analysis procedure for conducting an analysis in pure torsion. Completing the analysis broadly involves defining analysis parameters and member properties followed by an incremental analysis with nested iteration to satisfy equilibrium throughout the section.

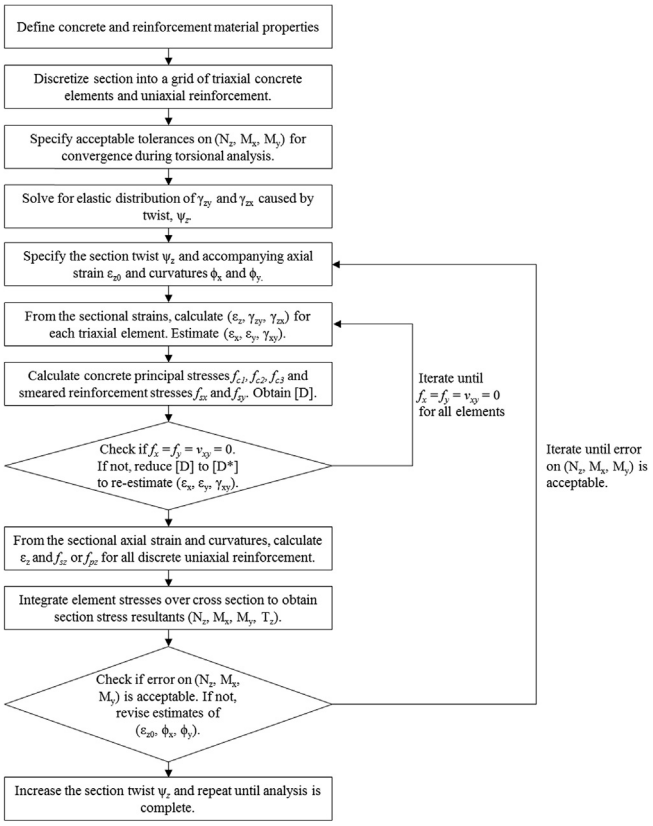

Fig. 8. Program flowchart for conducting an analysis of a member in pure torsion.

To begin the analysis, the user first needs to define the discretization of the section, material properties, smearing of the transverse reinforcement and the location of the longitudinal reinforcement. Convergence criteria are also needed to define the maximum acceptable error on N_z, M_x, and M_y which may occur while conducting a torque-twist analysis. For the analyses performed, tolerances of ±5 kN for axial load and ±5 kN m for the bending moments were deemed to be acceptable, though these tolerances may need to be reduced when modelling smaller members. Note that convergence for V_y and V_y is not checked since the strain distributions associated with γ_{zy0} and γ_{zx0} are not defined and hence not used.

Prior to beginning the sectional analysis of the reinforced concrete member, the shear strain distributions of γ_{zy} and γ_{zx} caused by twist need to be obtained from an elastic analysis using the method explained in Section 2.2.2. Once these distributions have been calculated, the torque-twist behaviour is computed by specifying the section twist, ψ_z, and varying the proportion of the axial strain, ε_{z0}, vertical curvature, ϕ_x, and lateral curvature, ϕ_y, to ensure that the only non-zero stress resultant is the torsion, T_z. If the error on N_z, M_x and M_y are larger than the allotted tolerances, new estimates of ε_{z0}, ϕ_x and ϕ_y are made until convergence is attained. Upon convergence, the load stage is deemed to be complete. The twist is incremented and the process repeats.

On the element level, the principal strains $(\varepsilon_1, \varepsilon_2, \varepsilon_3)$ are calculated using the set of strains $(\varepsilon_z, \gamma_{zy}, \gamma_{zx})$ from the sectional strains and an estimate of the distortion strains $(\varepsilon_x, \varepsilon_y, \gamma_{xy})$. The concrete and transverse reinforcement stresses are evaluated using the constitutive relationships presented in Section 2.3 and then the element stress vector $(f_x, f_y, f_z, v_{xy}, v_{zy}, v_{zx})$ and stiffness matrix $[D]$ are obtained. The distortion strains are then iteratively updated in order to ensure that $f_x = f_y = v_{xy} = 0$. Once this condition has been met, the process is repeated for each element in the cross section, after which the stresses are integrated to obtain the stress resultants N_z, M_x, M_y and T_z using the equations in Section 2.4. Note that treating the longitudinal reinforcement is analogous to working with the triaxial concrete elements but is simpler as they only carry a longitudinal stress f_z as a function of ε_z.

Although the model converges quite quickly in both the uncracked elastic stage and cracked elastic stages, a large amount of iteration is needed during moments of predominantly nonlinear behaviour (i.e. at the onset of cracking, when the reinforcement is yielding or when the concrete is crushing). It was also found that convergence on the axial load N_z is particularly sensitive to small variations in the longitudinal strain distribution and strongly influences the rate of convergence during an analysis.

3. Model validation

The proposed model was validated against 115 tests in pure torsion which were found in the literature, consisting of 108 reinforced concrete beams, 5 prestressed concrete beams and 2 reinforced concrete shell elements. Of the beams modelled, 23 were hollow with the remainder being solid. All members analyzed were rectangular in cross section and represent a wide spectrum of geometric and material configurations leading to different failure modes. In this section, a summary of predictions of ultimate torque is first presented, followed by a more thorough comparison of predicted and observed torque-twist behaviour for beams and shells in Sections 3.1 and 3.2 respectively.

Table 1 summarizes the experimental programs investigated in greater detail. Key parameters investigated by each series of experiments include geometric aspects (i.e. hollow vs. solid members, aspect ratio, size), quantity of longitudinal reinforcement, ρ_{long}, quantity of transverse reinforcement, ρ_{trans}, concrete cylinder

Table 1
Description of experimental programs. All dimensions are noted in mm.

Investigator	Description	# Tests	Investigator	Description	# Tests
Bernardo and Lopes (2009) [21]	High strength hollow reinforced concrete beams with a square cross section. *Size:* 600 × 600 f_c' = 46.2–94.8 MPa ρ_{long} = 0.28–2.41% ρ_{trans} = 0.15–1.36%	16	Koutchoukali and Belarbi (2001) [25]	High strength solid reinforced concrete beams with rectangular cross section. *Size:* 203 × 305 f_c' = 39.6–93.9 MPa ρ_{long} = 0.83–1.29% ρ_{trans} = 0.92–1.42%	9
Bruun and Bentz (2017) [22]	Reinforced concrete shell elements tested in pure torsion. *Size:* 1626 × 1626 × 286 f_c' = 30.4 & 37.6 MPa ρ_{long} = 2.95% ρ_{trans} = 1.95%	2	Mardukhi and Collins (1974) [26]	Hollow prestressed concrete beams investigating the interaction between torsion and bending. One test done in pure torsion. *Size:* 305 × 431 f_c' = 35.6 MPa ρ_{long} = 1.51% ρ_{trans} = 0.49%	1
Fang and Shiau (2004) [23]	Solid rectangular reinforced concrete beams. High strength (H-Series) and normal strength (N-Series) concrete. *Size:* 350 × 500 f_c' = 35.5–78.5 MPa ρ_{long} = 0.69–1.95% ρ_{trans} = 0.61–2.01%	16	Mitchell and Collins (1978) [27]	Solid and hollow reinforced and prestressed concrete beams. *Size:* Varied (360 × 430 typ.) f_c' = 29.6–38.9 MPa ρ_{long} = 0.35–3.88% ρ_{trans} = 0.68–0.80%	6
Hsu (1968) [24]	Comprehensive series of tests on rectangular cross sections. *Size:* Varied (254 × 381 typ.) f_c' = 14.3–45.8 MPa ρ_{long} = 0.40–3.16% ρ_{trans} = 0.40–3.20%	53	Rasmussen and Baker (1995) [28]	High strength solid reinforced concrete beams with rectangular cross section. *Size:* 160 × 275 f_c' = 36.3–109.8 MPa ρ_{long} = 3.47% ρ_{trans} = 1.49%	12

strength, f'_c, and amount of prestress. Note the following definitions of ρ_{long} and ρ_{trans}:

$$\rho_{long} = \frac{A_{s,long}}{A_{gross}} \tag{35}$$

$$\rho_{trans} = \frac{A_{s,trans} p_h}{A_{out} s} \tag{36}$$

where $A_{s,long}$ is the total cross sectional area of longitudinal reinforcement, $A_{s,trans}$ is the cross sectional area of one hoop of torsional reinforcement, p_h is the perimeter of the area enclosed by the centreline of the torsional reinforcement, s is the spacing of torsional reinforcement, A_{gross} is the gross cross sectional area of the member and A_{out} is the area enclosed by the outside perimeter of the member's cross section (i.e. for a solid rectangular section, $A_{gross} = A_{out}$). Although ρ_{long} is the conventional volumetric ratio of longitudinal steel to concrete, ρ_{trans} is the volumetric ratio of transverse reinforcement to the volume enclosed by the outside dimensions of the member, making it an appropriate metric for both solid and hollow members.

When performing the validation studies, each member's cross section was represented as a grid with approximately 1200–2000 elements across the cross section. When smearing the transverse reinforcement into the reinforced concrete elements, the steel was smeared from the outside surface of the member to the depth of the stirrup, which typically took place over four to six layers of elements. The steel was proportioned so that the area of steel assigned when calculating ρ increased linearly from a minimum in the elements in the outside layer to a maximum inside the layer of elements located at the depth of the stirrup (i.e. if a stirrup with cross sectional area of 100 mm^2 was smeared over four layers of elements, the area was distributed as 10 mm^2 in the exterior layer and increasing to 40 mm^2 in the interior layer). Apart from the process of selecting an appropriate discretization of the member and smearing the transverse reinforcement accordingly, no additional model calibration was done to get the presented results. The complete torque-twist response was obtained for each member using an analysis over 250–300 load steps, taking a total of around 2–3 min each.

Table 2 contains a summary of results for each of the 115 specimens modelled, including the experimentally observed ultimate torque, $T_{ult,Test}$, the ultimate torque as predicted by the proposed model, $T_{ult,Pred}$, and the ratio of the test value to the predicted value, T_{Test}/T_{Pred}. From the results, it can be seen that the model gives consistently good predictions of peak torque, with an average test to predicted ratio of 1.028 and a coefficient of variation of 13.30%. The quality of predictions for each of the 8 experimental investigations is high, with the exception of the highly reinforced, high-strength beams tested by Rasmussen and Baker which are generally overestimated by the model.

Fig. 9 shows the results shown in Table 2 plotted against concrete cylinder strength, aspect ratio, quantity of transverse reinforcement and quantity of longitudinal reinforcement. It can be seen that predictions of ultimate torque are fairly independent of quantity of longitudinal and transverse reinforcement, performing well for both very low amounts of reinforcement (typically resulting in failure caused by yielding of the reinforcement) as well as very large amounts of reinforcement (typically resulting in failure caused by crushing of the concrete before yielding of the steel). The model also performed well over a variety of aspect ratios, a parameter which strongly influences the distribution of shear stresses caused by torsion, providing further validation for the method of determining the shear strain distribution caused by torsion previously described in Section 2.2.2. With regards to the effect of concrete strength on the predictions, the model appears to work well for both normal and high strength concrete. But as noted earlier, the relatively poor results for the tests by Rasmussen and Baker contribute to the poor predictions for specimens whose concrete strength is over 100 MPa.

The model also works equally well for both hollow and solid sections, which is not evident from Fig. 9. Considering the 23 hollow beams tested by Bernardo and Lopes (16), Hsu (4), Mardukhi and Collins (1) and Mitchell and Collins (2), the average test/pred ratio is 1.029 and a coefficient of variation of 9.60%.

Table 2
Summary of analysis results.

Investigator	Specimen	$T_{ult,Test}$ [kNm]	$T_{ult,Pred}$ [kNm]	T_{Test}/T_{Pred}	Investigator	Specimen	$T_{ult,Test}$ [kNm]	$T_{ult,Pred}$ [kNm]	T_{Test}/T_{Pred}
Bernardo and Lopes (2009)	A-48.4-0.37	150.78	125.4	1.203	Hsu (1968) (con't)	I2	36.0	33.3	1.083
	A-47.3-0.76	254.77	236.6	1.077		I3	45.6	46.3	0.985
	A-46.2-1.00	299.91	280.8	1.068		I4	58.1	54.8	1.059
	A-54.8-1.31	368.22	356.1	1.034		I5	70.7	65.8	1.075
	A-53.1-1.68	412.24	388.7	1.061		I6	76.7	72.4	1.060
	B-75.6-0.30	115.95	97.3	1.192		J1	21.5	20.2	1.063
	B-69.8-0.80	273.28	251.8	1.085		J2	29.2	24.7	1.178
	B-77.8-1.33	355.85	413.0	0.862		J3	35.3	30.3	1.165
	B-79.8-1.78	437.85	445.4	0.983		J4	40.7	33.2	1.226
	B-76.4-2.20	456.19	462.4	0.986		G1	26.8	21.4	1.250
	C-91.7-0.37	151.76	120.2	1.263		G2	40.3	34.0	1.186
	C-94.8-0.76	266.14	238.7	1.115		G3	49.6	49.4	1.005
	C-91.6-1.29	351.16	416.1	0.844		G4	64.9	62.4	1.040
	C-91.4-1.71	450.31	469.0	0.960		G5	72.0	70.5	1.021
	C-96.7-2.07	467.26	516.9	0.904		G6	39.1	33.4	1.171
	C-87.5-2.68	521.33	543.9	0.959		G7	52.7	51.1	1.031
Bruun and Bentz (2017)	ES1	132.40	132.7	0.998		G8	73.4	65.9	1.114
	ES2	177.10	180.2	0.983		N1	9.1	7.5	1.208
Fang and Shiau (2004)	H-06-06	92.0	89.1	1.033		N1a	9.0	7.5	1.204
	H-06-12	115.1	109.7	1.050		N2	14.5	12.5	1.154
	H-12-12	155.3	146.3	1.062		N2a	13.2	12.3	1.075
	H-12-16	196.0	163.7	1.198		N3	12.2	10.9	1.124
	H-20-20	239.0	202.3	1.181		N4	15.7	13.4	1.173
	H-07-10	126.7	111.6	1.135	Koutchoukali and Belarbi (2001)	B5UR1	19.4	20.2	0.961
	H-14-10	135.2	139.6	0.969		B7UR1	18.9	19.9	0.952
	H-07-16	144.5	122.5	1.179		B9UR1	21.1	20.6	1.025
	N-06-06	79.7	68.4	1.166		B12UR1	19.4	21.2	0.916
	N-06-12	95.2	74.4	1.280		B14UR1	21.0	19.8	1.060
	N-12-12	116.8	99.3	1.177		B12UR2	18.4	21.6	0.854
	N-12-16	138.0	112.1	1.231		B12UR3	22.5	24.8	0.906
	N-20-20	158.0	125.7	1.257		B12UR4	23.7	27.7	0.856
	N-07-10	111.7	87.3	1.279		B12UR5	24.0	38.0	0.631
	N-14-10	125.0	103.6	1.206		B5UR1	19.4	20.2	0.961
	N-07-16	117.3	95.4	1.230	Mardukhi and Collins (1974)	TB4	64.8	64.1	1.011
Hsu (1968)	B1	22.3	20.5	1.086					
	B2	29.3	29.4	0.997	Mitchell and Collins (1978)	P1	81.9	80.3	1.020
	B3	37.5	37.1	1.010		P2	80.8	82.0	0.985
	B4	47.3	44.0	1.075		P3	53.1	53.0	1.002
	B5	56.2	56.4	0.995		P5	112.4	115.5	0.973
	B6	61.7	60.5	1.020		P6	89.3	89.7	0.996
	B7	26.9	28.4	0.948		PT4	65.4	64.0	1.022
	B8	32.5	32.8	0.991	Rasmussen and Baker (1995)	B30.1	16.62	19.2	0.864
	B9	29.8	30.1	0.990		B30.2	15.29	18.2	0.842
	B10	34.3	34.7	0.989		B30.3	15.25	17.5	0.870
	D1	22.4	21.5	1.042		B50.1	19.95	24.6	0.811
	D2	27.7	28.4	0.973		B50.2	18.46	23.5	0.787
	D3	39.1	38.9	1.004		B50.3	19.13	24.6	0.779
	D4	47.9	45.9	1.044		B70.1	20.06	28.3	0.709
	M1	30.4	29.5	1.032		B70.2	20.74	28.1	0.738
	M2	40.6	38.4	1.057		B70.3	20.96	26.0	0.806
	M3	43.8	43.0	1.019		B110.1	24.72	35.3	0.701
	M4	49.6	49.1	1.011		B110.2	23.62	34.5	0.685
	M5	55.7	55.4	1.005		B110.3	24.77	34.5	0.718
	M6	60.1	60.5	0.993					
Mean Test/Pred									1.028
Coefficient of Variation									13.30%

3.1. Comparison of predicted torque-twist response with experimental data for beams

To validate the ability of the proposed model to capture the complete torque-twist behaviour of a reinforced concrete member in pure torsion, the predicted torque-twist response was compared with experimental data obtained by the P-series tested by Mitchell and Collins. The predicted and observed behaviour of four representative specimens, P1, P2, P3 and P6 are shown in Fig. 10. These selected specimens represent instances where the torsional behaviour is governed by several different factors: prestressing (P1, P2, P3), the presence of a hole in the cross section (P2), crushing of the concrete following yield of the transverse reinforcement (P6), and crushing of the concrete following yielding of both directions of reinforcement (P1, P2, P3).

For all four plots in Fig. 10, there is excellent agreement regarding the uncracked stiffness, gradual loss in stiffness following yielding and ultimate torque. Even P6, which has a softer predicted response than experimentally observed has a similar post-yielding tangent stiffness as the experiment, albeit occurring at a larger twist. The model was able to capture the response of both P1 and P2 (P2 being a hollow version of P1), and even captured the small increase in torsional strength due to the slightly larger amount of prestress. The simultaneous yielding of the transverse

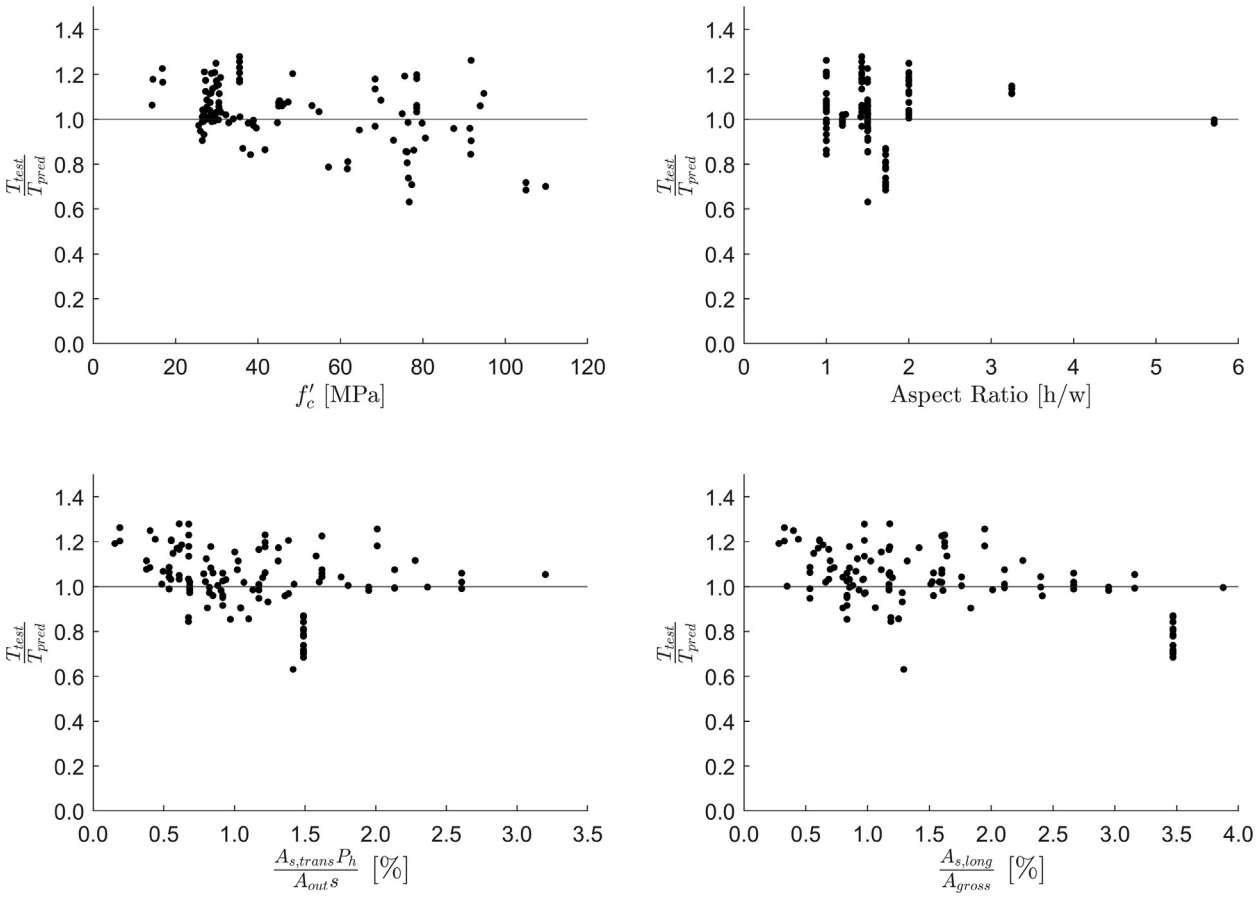

Fig. 9. Summary of results for specimens modelled, plotted against concrete strength, f'_c (top left), aspect ratio (top right), quantity of transverse reinforcement ρ_{trans} (bottom left) and quantity of longitudinal reinforcement ρ_{long} (bottom right).

and longitudinal steel in P3 was also well-captured by the model, and the post-yielding behaviour exhibited excellent agreement with the experimental observations.

The choice of constitutive modelling, particularly the assumption of no tensile stresses in the cracked concrete, has resulted in some discrepancies in the predictions and the experiments. The model tends to consistently under-predict the cracking torque of the members. The reason for this is because the small post-cracking tensile stresses in plain concrete, as well as the more significant post-cracking tensile stresses in reinforced concrete (tension softening and tension stiffening respectively) are ignored. Although this is not inherently the fault of the proposed framework, it does suggest that a more sophisticated model for tension in concrete is needed to adequately predict the cracking torque of a member.

Neglecting tension stiffening when modelling reinforced concrete beams also leads to a large discrepancy in the torque-twist response shortly after cracking and can be seen in all four plots shown in Fig. 10. The effect of neglecting tension stiffening is particularly noticeable for P6, a heavily reinforced beam with ρ_{long} = 3.88% and ρ_{trans} = 0.68%. Although the cracking torque is well-predicted by the model ($T_{cr,\exp}$ = 25.4 kN m and $T_{cr,pred}$ = 26.6 kN m), the reduction in torsional stiffness was overestimated to be a loss of 90%, compared to an experimentally observed reduction of about 60%, which is hardly noticeable in the torque-twist plot in the figure.

The discrepancy caused by ignoring post-cracking tensile stress in the concrete disappears following yielding of both the longitudinal and transverse steel (like in P1, P2 and P3). When this occurs, the tensile stresses in the concrete go to zero, as they are limited by local behaviour of the steel yielding at the crack. In instances such as P6, where only the transverse steel yields, the discrepancy remained until the global behaviour was governed by crushing of the concrete. Although neglecting tension stiffening leads to conservative estimates of the cracking torque and underpredicts the post-cracking stiffness, the overall framework is still able to give good results using the constitutive models discussed in this paper. Further improvements to address the highlighted shortcomings can be addressed by using different constitutive relationships for post-cracking behaviour.

3.2. Comparison of predicted torque-twist response with experimental data for shells

Two reinforced concrete shell elements tested by Bruun in 2017 were also used to validate the numerical model for shells [22]. These shell elements, measuring 1626 mm by 1626 mm and 285 mm thick, were tested in displacement control in pure torsion using the Shell Element Tester at the University of Toronto. The ES series represents the first set of shell tests to have been performed in pure torsion and displacement control, and hence provide valuable peak and post-peak data to be used in this validation exercise. These specimens were heavily reinforced diagonally and were loaded in biaxial bending in-plane. As the longitudinal reinforcement was rotated 45° to this axis, the applied moments resulted in torsion on the specimens on a diagonal plane aligned with the reinforcing steel. More details of the loading and observed behaviour can be found in Bruun and Bentz [22] and Bruun [29].

When modelling the specimens, a mesh similar to the one shown in Fig. 3 was adopted, representing a diagonal slice through

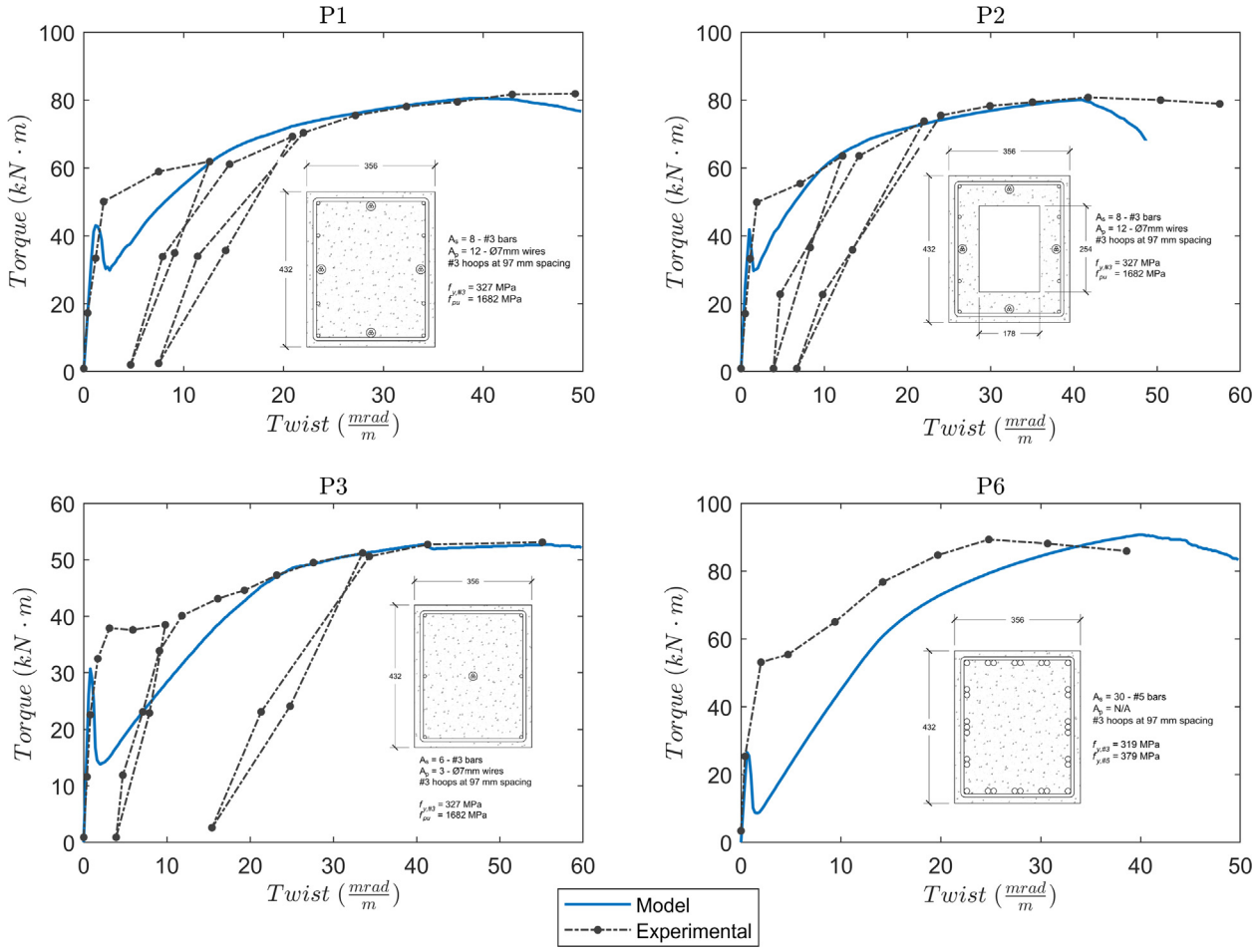

Fig. 10. Comparison of predicted and observed torque-twist behaviour for specimens P1 (top left) and P2 (top right), P3 (bottom left) and P6 (bottom right).

the shell. A 1 m strip was modelled, and the torque per unit length of the strip was used to compare the predictions with the experimental results. The validity of using a unit length and comparing its response with that of a larger specimen, is confirmed by considering the ratio of shear stresses of the long side to the short side when performing an elastic analysis of a rectangle. For the 285 mm thick shell, a 1 m slice has an aspect ratio of 3.5 – elastic theory states that the shear stresses along the long face are

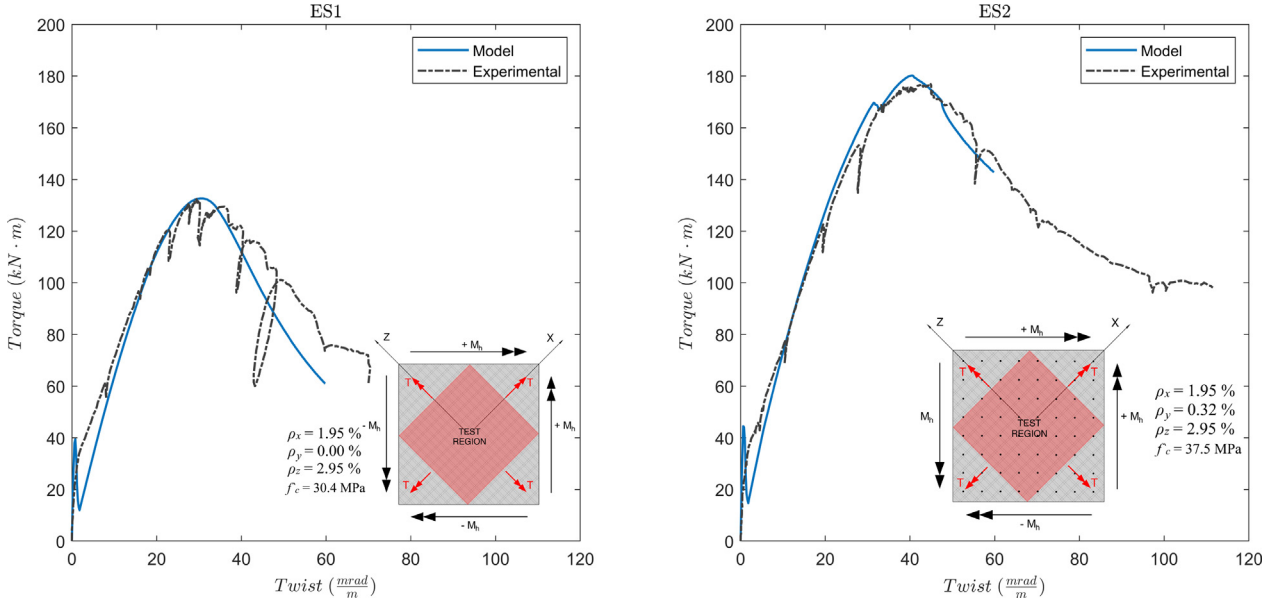

Fig. 11. Predicted and observed torque-twist behaviour for ES1 (left) and ES2 (right) shell elements.

approximately 5 times larger than those on the short face. This ratio approaches infinity rapidly for larger aspect ratios, suggesting that the torsional behaviour of a continuous shell is dominated by the shear stresses carried along its faces, as opposed to those carried through the thickness. For modelling purposes, this means that comparing the normalized torsion along the length of the long face is an appropriate approach for modelling the torque-twist response of larger shell structures.

Table 3
Model validation – Mardukhi prestressed concrete torsion and bending (TB) series.

No.	Name	$T_{ult,test}$ [kNm]	$M_{ult,test}$ [kNm]	$T_{ult,pred}$ [kNm]	$M_{ult,pred}$ [kNm]	Test/Pred
1	TB1	62.4	73	63.1	74	0.989
2	TB2	53.2	157	56.3	165	0.945
3	TB3	27.8	193	28.7	199	0.969
4	TB4	64.8	0	64.1	0	1.011
5	TB5	0	237	0	239	0.992
Average						0.981
Coefficient of Variation						2.29%

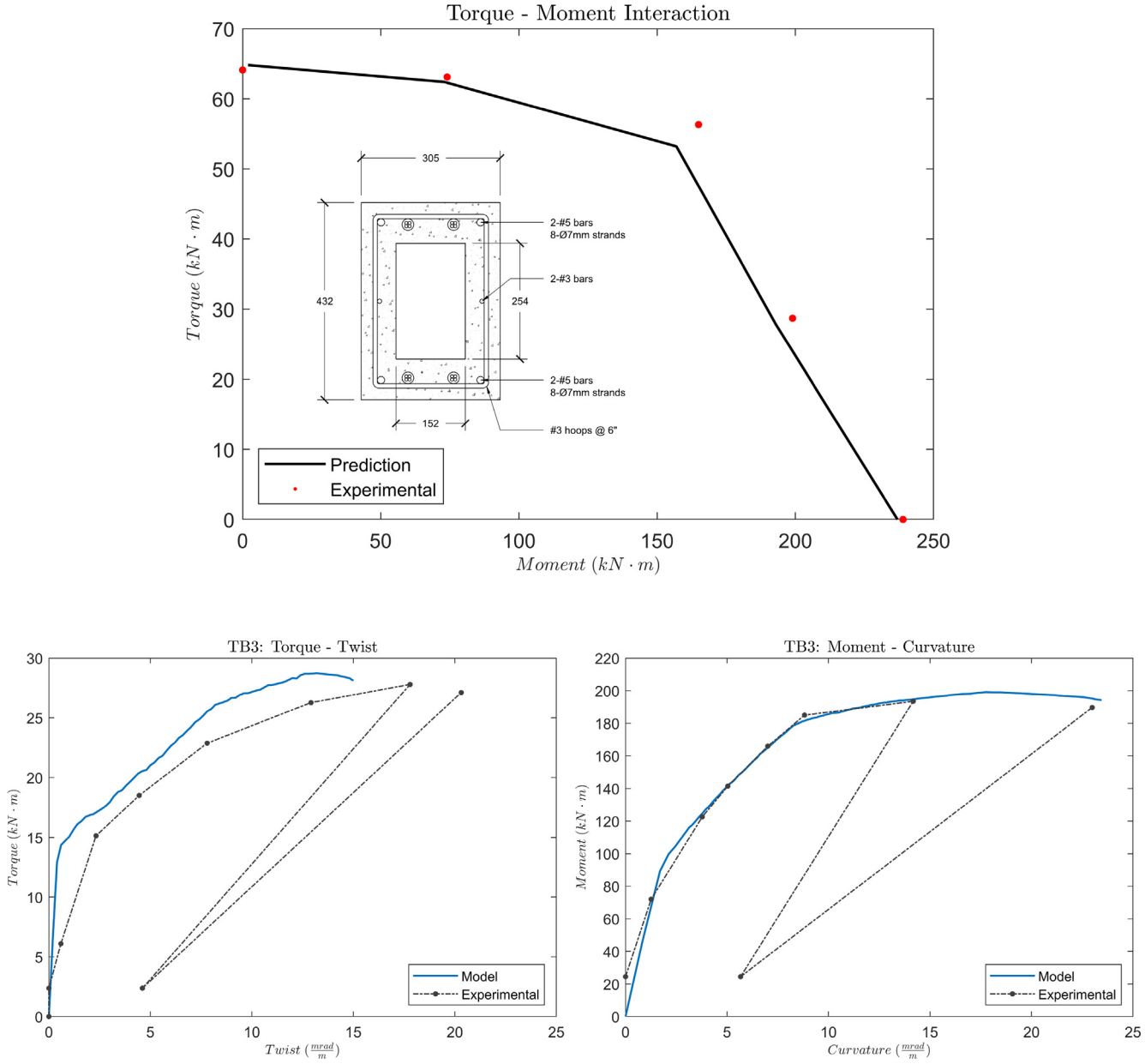

Fig. 12. Predicted and observed behaviour for combined bending and torsion. Torsion-bending interaction for the Mardukhi's TB series (top) and torque-twist (bottom left) and moment-curvature plots for beam TB3 (bottom right).

Fig. 11 shows both the experimental and predicted torque-twist response for shells ES1 and ES2, which were nominally identical except ES2 contained T-headed reinforcement through the thickness and had a slightly higher f_c'. Excellent agreement can be seen between the predicted and experimentally observed behaviour, particularly the post-cracking stiffness, peak torque and ultimate twist. Although there is a discrepancy between the predicted and observed behaviour shortly after cracking due to tension stiffening being neglected, the overall behaviour was well-captured because failure was dominated by crushing of the concrete prior to yielding of *x*- or *z*- direction reinforcement.

4. Extension to torsion and bending – preliminary validation

Although Section 2.2.2 mentions that the shear strain distribution caused by twist obtained from a linear elastic analysis of the cross section does not stay the same in cases of combined torsion and bending of cracked reinforced concrete members, preliminary validation has shown that using the elastic shear strain distribution for a combined torsion-bending analysis still allows for good predictions of torque-twist and moment-curvature response to be made. A series of validation studies were conducted to see how well this approach worked using the Marduhki series of symmetrically reinforced prestressed concrete beams subjected to combined torsion and bending [26]. The results of this study are shown in Table 3 and Fig. 12, where the torsion-bending interaction is predicted with excellent accuracy, and good agreement is obtained between the measured and predicted torque-twist and moment-curvature behaviour.

When modelling these beams using the methodology outlined in this paper, the use of the elastic shear strain distribution caused by twist led to large unbalanced shear forces in the member during the analysis. These unbalanced forces are due to the differences in the distribution of stiffnesses in the member following flexural cracking. For an uncracked rectangular member, the shear strain distribution caused by twist is symmetric about both the x- and y- axes. Following cracking however, the stiffnesses and hence the distribution of shear strains is no longer symmetric about both directions as the flexural tension side is cracked and the flexural compression side may be uncracked. Applying the elastic shear strain distribution to this system hence leads to a non-zero shear force carried by the section in addition to the applied torsion and moment. Despite this issue however, reasonable predictions of strength, as well as torque-twist and moment-curvature response were obtained by using the elastic shear strain distribution. Further work is needed to model torsion in combination with bending and shear to address this issue in a more rigorous manner.

5. Conclusions and areas of future work

In conclusion, a sectional analysis tool is presented for the nonlinear analysis of reinforced and prestressed concrete members subjected to pure torsion. A key component of the methodology is using the elastic shear strain distribution caused by twist to obtain the complete torque-twist behaviour. The resulting model is thus able to describe detailed sectional behaviour under torsion in a computationally efficient manner, combining the strengths of existing finite element and space-truss models available in the literature. Although the methodology has been implemented for modelling pure torsion in rectangular cross sections using select constitutive relationships for concrete and steel, the framework is general enough to permit the use of any constitutive models and be extended to account for any combinations of axial load, shear, moment and torsion being carried by an arbitrarily-shaped cross section.

A validation exercise using 115 specimens tested in pure torsion found in the literature were modelled using the proposed analysis method to evaluate its predictive ability. The average test to predicted ratio for ultimate torque was found to be 1.028, with a coefficient of variation of 13.30%. Excellent predictions of both the peak load and overall torque-twist behaviour of specimens were made, both of which are important properties when considering Equilibrium Torsion and Compatibility Torsion in actual structures. Other positive features of the model are its fast runtime compared to performing a 3-D nonlinear finite element analysis and its limited calibration requirements, both of which enhance its practical appeal.

Areas of future work include the following:

- Validating the approach for arbitrarily shaped cross sections. Although the shear strain distributions presented in Fig. 4 suggest that the current approach can be extended to T-beams, comparison with experiments in the literature are required to validate this hypothesis.
- Obtaining a means to calculate the shear strain distributions for γ_{zy0} and γ_{zx0} which are associated with the stress resultants V_y and V_x respectively to have a complete set of strain distributions for the six sectional strains.
- Expanding the capabilities of the model to account for combinations of axial load, shears, moments and torsion. This primarily involves developing a means to calculate the changes in warping as the member cracks under load.
- Improving the constitutive model for cracked reinforced concrete in tension. The current approach leads to underestimating the stiffness following cracking and is less appropriate for members containing very small amounts of transverse reinforcement.

This work is a promising first step towards efficient sectional analysis for members subject to torsion and further improvements would provide engineers with a practical tool to model members subjected to complex loading combinations and understand the fundamental mechanisms which allow them to carry load.

Acknowledgements

The authors would like to acknowledge the support of the Natural Sciences and Engineering research Council of Canada (NSERC) [funding reference number 518446].

References

[1] Collins MP, Lampert P. Redistribution of moments at cracking - the key to simpler torsion design. In: American Concrete Institute Special Publication, SP-35; 1973. p. 343–83.
[2] Vecchio FJ, Selby RG. Towards compression-field analysis of reinforced concrete solids. J Struct Eng 1991;117(6):1740–58.
[3] Bairan JM, Mari AR. Coupled model for the nonlinear analysis of anisotropic sections subjected to general 3D loading. Part 2: implementation and validation. Comput Struct 2006;84(31–32):2264–76.
[4] Capdevielle S, Grange S, Dufour F, Desprez C. A multifier beam model coupling torsional warping and damage for reinforced concrete structures. Eur J Environ Civ Eng 2016;20(8):914–35.
[5] Navarro-Gregori J, Miguel Sosa P, Fernández Prada MA, Filippou FC. A 3D numerical model for reinforced and prestressed concrete elements subjected to combined axial, bending, shear and torsion loading. Eng Struct 2007;29:3404–19.
[6] Bentz EC. Sectional analysis of reinforced concrete members Ph.D. thesis. Department of Civil Engineering, University of Toronto; 2000.
[7] Vecchio FJ, Collins MP. The modified compression-field theory for reinforced concrete elements subjected to shear. ACI J 1986;83(22):219–31.
[8] Rahal KN, Collins MP. Analysis of sections subjected to combined shear and torsion – a theoretical model. ACI Struct J 1995;92(44):459–69.
[9] Jeng CH, Hsu TTC. A softened membrane model for torsion in reinforced concrete members. Eng Struct 2009;31(9):1944–54.
[10] Greene G, Belarbi A. Model for reinforced concrete members under torsion, bending, and shear. I: Theory. J Eng Mech 2009;135(9):961–9.

[11] Bernardo LFA, Andrade JMA, Lopes SMR. Modified Variable Angle Truss-Model for torsion in reinforced concrete beams. Mater Struct 2012;45(12):1877–902.
[12] Hooke R. Lectures De Potentia Restitutiva or of Spring Explaining the Power of Springing Bodies. London: Royal Society; 1678.
[13] Timoshenko SP, Goodier JN. Theory of elasticity third edition. McGraw-Hill; 1970. p. 551.
[14] Collins MP, Mitchell D. Prestressed concrete structures. Englewood Cliffs: Prentice Hall; 1991. p. 766.
[15] Cook RD. Finite element concepts and applications. 2nd Ed. New York, N. Y.: John Wiley and Sons; 1991.
[16] Popovic S. A review of stress-strain relationships for concrete. ACI J 1970;67 (3):243–8.
[17] Porasz A. An investigation of the stress-strain characteristics of high-strength concrete in shear M.A.Sc. Thesis. Department of Civil Engineering, University of Toronto; 1989.
[18] Bentz EC. Explaining the riddle of tension stiffening models for shear panel experiments. J Struct Eng 2005;131(9):1422–5.
[19] Proestos GT. Modelling reinforced and prestressed concrete structures subjected to shear and torsion Ph.D Thesis. Department of Civil & Mineral Engineering, University of Toronto; 2018.
[20] Hrynyk TD. Behaviour and modelling of reinforced concrete slabs and shells under static and dynamic loads Ph. D. Thesis. Department of Civil Engineering, University of Toronto; 2013.
[21] Bernardo LFA, Lopes SMR. Torsion in high-strength concrete hollow beams: strength and ductility analysis. ACI Struct J 2009;106(1):39–48.
[22] Bruun EPG, Bentz EC. Experimental procedures for displacement- torsion tests on reinforced concrete shells. In: Proceedings from the 7th international conference on advances in experimental structural engineering. Pavia, Italy; 2017.
[23] Fang IK, Shiau JK. Torsional behaviour of normal- and high-strength concrete beams. ACI Struct J 2004;101(3):304–13. May-June.
[24] Hsu Thomas TC. Torsion of structural concrete - behavior of reinforced concrete rectangular members. In: Torsion of Structural Concrete, SP-18, American Concrete Institute, Detroit; 1968. p. 261–306.
[25] Koutchoukali NE, Belarbi A. Torsion of high-strength reinforced concrete beams and minimum reinforcement requirement. ACI Struct J 2001;98 (4):462–9.
[26] Mardukhi J. The behaviour of uniformly prestressed concrete box beams in combined torsion and bending. M.A.Sc. Thesis; 1974, 72 pp.
[27] Mitchell D, Collins MP. Influence of prestressing on torsional response of concrete beams. J Prestressed Concr Instit 1978;23(3):54–73.
[28] Rasmussen LJ, Baker G. Torsion in reinforced normal and high-strength concrete beams – Part 1: experimental test series. ACI Struct J 1995;92 (1):56–62.
[29] Bruun EPG. The hybrid panel-truss element: developing a novel finite element for the nonlinear analysis of reinforced concrete beams and shells M.A.Sc thesis. Department of Civil and Mineral Engineering, University of Toronto; 2017.